Biphase Ordering of Iron Oxide Surfaces

N. G. Condon,[1] F. M. Leibsle,[1] A. R. Lennie,[2] P. W. Murray,[1] D. J. Vaughan,[2] and G. Thornton[1,*,†]
[1] *Interdisciplinary Research Centre in Surface Science, University of Liverpool, Liverpool L69 3BX, United Kingdom*
[2] *Department of Geology, The University of Manchester, Oxford Road, Manchester M13 9PL, United Kingdom*

(Received 7 April 1995)

Scanning tunneling microscopy and low energy electron diffraction have been used to study the α-$Fe_2O_3(0001)$ surface in an ultrahigh vacuum. Our results show that this surface can be stabilized by coexisting α-$Fe_2O_3(0001)$ and FeO(111) phases, with each phase existing in atomically well-ordered islands of mesoscopic dimensions. Furthermore, the islands themselves are arranged to form a superlattice. The formation of this superlattice can be explained in terms of the lattice mismatch between two types of oxygen sublattices.

PACS numbers: 61.16.Ch, 61.14.Hg, 68.35.Bs, 68.55.Nq

A knowledge of the surface science of iron oxides is a prerequisite for understanding the role of these materials in catalysis and corrosion, and there is also considerable interest in their magnetic properties. Despite the obvious importance of these materials, to date there have been few surface science studies of either α-Fe_2O_3 or Fe_3O_4 single crystal surfaces [1–9]. The bulk thermodynamic Fe-O phase diagram is relatively complicated, with several easily interchangeable iron oxide phases [10]. Previous studies of α-$Fe_2O_3(0001)$ have shown that its surface phase diagram is also complex, with surface compositions being highly dependent on the manner of preparation [1–5,8,9]. In part, this arises because a close-packed oxygen layer lies parallel to α-$Fe_2O_3(0001)$, making it crystallographically similar to $Fe_3O_4(111)$ and FeO(111), as shown in Fig. 1. This similarity facilitates epitaxial growth of one phase upon another. Indeed, it has been shown possible to terminate α-$Fe_2O_3(0001)$ with a thin layer of $Fe_3O_4(111)$ [1–3], while other results were consistent with an FeO(111) termination [2,3].

In this Letter we present STM images recorded from an α-$Fe_2O_3(0001)$ surface which reveal a new form of surface reconstruction. The images show that the surface is stabilized by the coexistence of mesoscopic islands of two iron oxide phases, α-$Fe_2O_3(0001)$ and FeO(111), with the islands themselves arranged to form a superlattice. The images are consistent with low energy electron diffraction (LEED) patterns from these surfaces. In particular, they show that additional LEED beams result from the long-range order of the superlattice, rather than the multiple scattering across an interface with which they have previously been associated [2].

Our experiments were performed using a commercial ultrahigh vacuum scanning tunneling microscopy (STM) (Omicron GmbH), with the α-$Fe_2O_3(0001)$ sample being prepared by cycles of argon ion bombardment and annealing to 800 °C. The final anneal was carried out in 1×10^{-6} mbar O_2. This sample preparation is similar to that employed in previous studies of α-$Fe_2O_3(0001)$ [2–4]. The unit cell directions of the α-$Fe_2O_3(0001)$ substrate were obtained by reference to STM images of an $Fe_3O_4(111)$ selvedge [1].

The surfaces formed in this way were first examined with LEED, revealing a pattern which at first sight appears to be representative of a $\sqrt{3} \times \sqrt{3}R30°$ reconstruction. All of the LEED beams were "floreted," being surrounded by smaller spots having hexagonal symmetry. This type of α-$Fe_2O_3(0001)$ LEED pattern was reported in Refs. [2] and [3]. The first observation of floreted LEED patterns from epitaxially grown structures dates back to the beginning of modern surface science, being explained on the basis of multiple scattering across interfaces [11]. In the case of the α-$Fe_2O_3(0001)$ LEED pattern, the LEED symmetry and spot splitting has been rationalized on the basis of a thin FeO(111) layer forming the selvedge [2,3].

STM images of these surfaces, however, reveal a fascinating and complex surface topography, as illustrated in Fig. 2(a). Two different structures appear to coexist in the form of small islands on the surface. The islands themselves are arranged to form an additional long-range periodicity. Figure 2(b) shows a high resolution image of the surface. We note that the islands appear in two

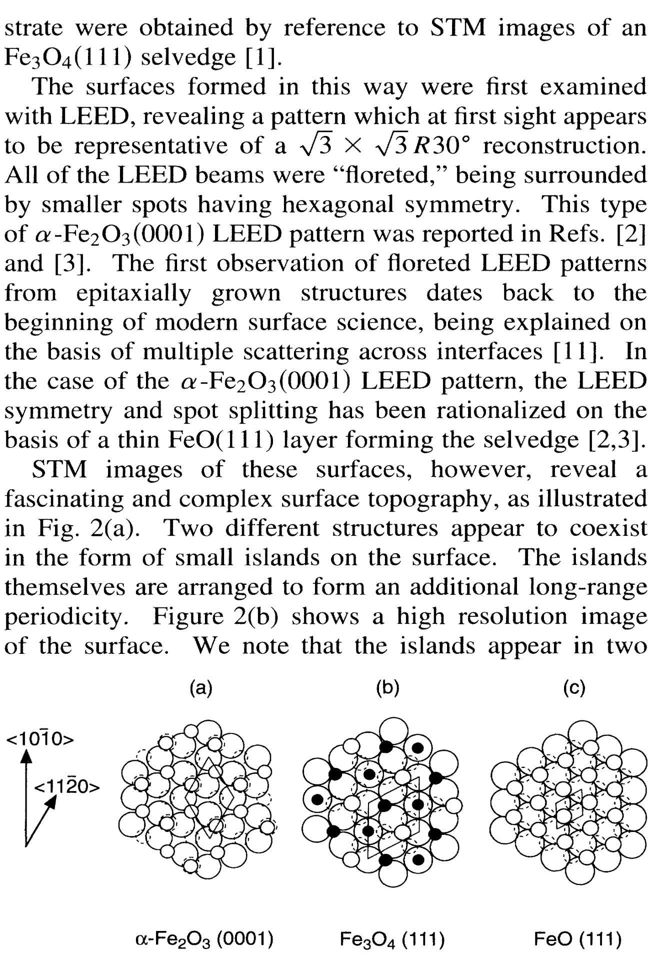

FIG. 1. Surface periodicities of iron oxides obtained by a lattice projection of iron oxide structures. The surface unit cell constants are (a) 5.03, (b) 5.92, and (c) 3.04 Å [12,13]. Octahedrally coordinated Fe atom positions above (small open circles) and below (dashed open circles) on either side of the close packed O layers (large open circles) are shown. In the $Fe_3O_4(111)$ structure the tetrahedral Fe^{3+} sites are shown as solid circles. The lattice directions appropriate to α-$Fe_2O_3(0001)$ are indicated.

0031-9007/95/75(10)/1961(4)$06.00

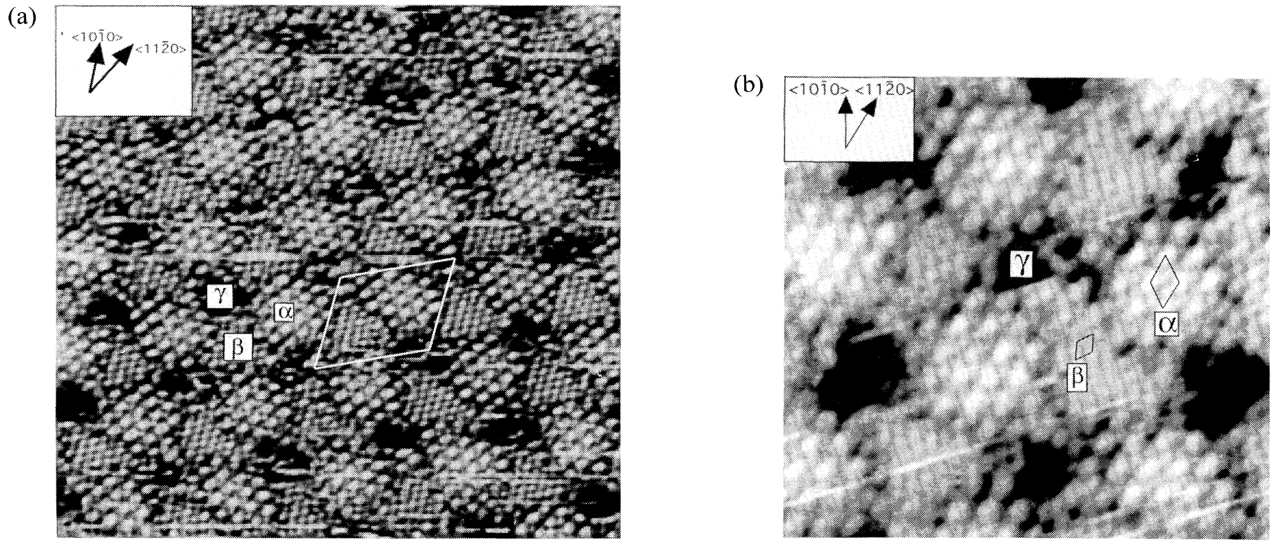

FIG. 2. (a) A 200 × 200 $Å^2$ constant current (sample bias -2 V, tunneling current 1 nA) STM image of an α-Fe_2O_3(0001) surface after preparation as described in the text. This image shows two types of islands, labeled α and β, with holes at positions labeled γ. The islands are ordered, forming a hexagonal superlattice. The unit cell of the superlattice, which is indicated, has a characteristic dimension of 40 ± 5 Å and is rotated by 30° from the α-Fe_2O_3(0001) lattice. Corrugations across the α and β phases are measured to be 0.5 and 0.3 Å, respectively, and γ-region holes are 2.0 ± 0.5 Å deep relative to the surrounding terraces. The crystallographic directions of the α-Fe_2O_3(0001) substrate are indicated. Vertical and horizontal distances were calibrated using an image of Cu(110)-(2 × 1)-O which contained monatomic steps, for which the dimensions are known [16]. (b) A high resolution 80 × 80 $Å^2$ constant current (sample bias -2 V, tunneling current 1 nA) STM image of the same surface as that imaged in (a). The unit cells of the α and β phases are indicated. Atoms at the edge of the α-phase unit cell are imaged as bright features, with two weaker features just discernible within the unit cell. This contrast could arise from either an electronic effect or from surface relaxation within the island. The α-phase islands contain 18 ± 4 bright features, while the β phase contains 25 ± 6. The unit cell directions of the α-Fe_2O_3(0001) substrate are shown.

forms, with each possessing a different shape and internal periodicity. Islands are observed which are approximately circular in shape and have an internal periodicity of about 5 Å. Triangularly shaped islands with an internal periodicity of about 3 Å can also be distinguished. We designate these phases as α and β, respectively, and note that the unit cells of both phases are rotated by 30° with respect to each other. Areas appearing as "holes" are designated as γ.

In the α phase, both the periodicity and the alignment of the features relative to the crystallographic axes are consistent with imaging oxygen atoms at the surface of α-Fe_2O_3(0001)-(1 × 1), although we cannot rule out a contribution from Fe atoms. As for the β phase, we note that the ratio of unit cell lengths of the α and β phases is 1.61. This is close to the value (1.65) expected [13] if the β phase was comprised of FeO(111)-(1 × 1) islands, an assignment which is also consistent with the relative orientation of the unit cells. While we can identify the β phase with FeO(111), we have no means of determining whether the STM features correspond to Fe or O atoms, since the sublattices have the same periodicity.

Additional support for these assignments of the α and β phases comes from a careful examination of the corresponding LEED pattern, an example of which is shown in Fig. 3(a). Part of the overall symmetry, outlined by a dashed line, comes from the first-order beams expected from α-Fe_2O_3(0001)-(1 × 1). Another part of the overall symmetry, highlighted by a full line, indicates the presence of a structure coexisting on the surface with a unit cell which is rotated by 30° from that of α-Fe_2O_3(0001)-(1 × 1), and which is smaller by a factor of 1.62. Hence the LEED results are consistent with the formation of FeO(111) islands.

Fast Fourier transforms (FFT) can be used to convert a real space STM image into reciprocal space and to facilitate a comparison with the corresponding LEED pattern. An FFT of Fig. 2(a), shown in Fig. 3(b), clearly shows both the hexagonal symmetry and the floreting evident in the LEED pattern. Since an STM image is surface specific, the FFT is a reciprocal space representation of the uppermost layer(s) of the surface. In comparison, the probing depth of LEED is several layers. Since LEED floreting is mimicked in the FFT, we conclude that it is a direct result of the formation of a superlattice which involves long-range ordering of the islands and not the result of multiple scattering across an interface. We term this new and previously unanticipated phenomenon *biphase ordering*. Such ordering superficially resembles the well-known dimer–adatom–stacking-fault (DAS) reconstruction of Si(111)-(7 × 7) [14], with the faulted and unfaulted halves of the unit cell being the two phases. However, the

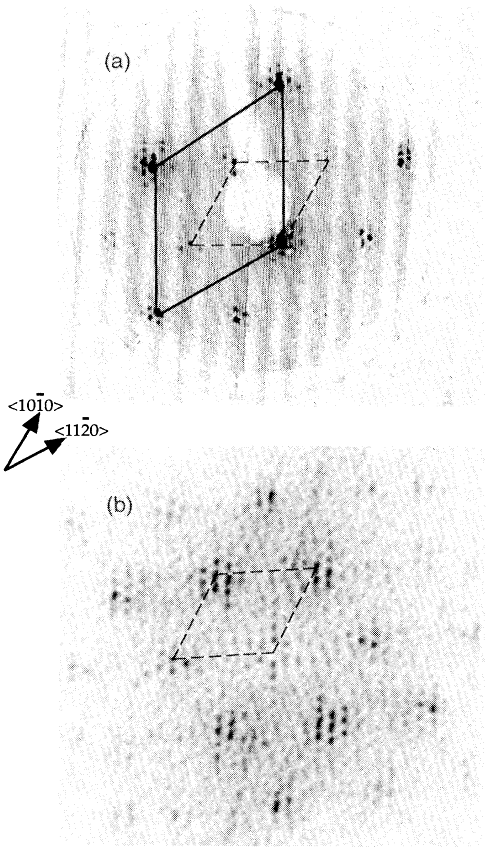

FIG. 3. (a) A LEED pattern of the surface imaged in Fig. 2, recorded at a primary beam energy of 58 eV. It was recorded off-normal incidence to reveal the zero order beam. The LEED pattern is a superposition of two symmetries, one arising from α-$Fe_2O_3(0001)$-1×1 (dashed line), the other from FeO(111)-1×1 (solid line). All the beams are floreted, being split into small hexagons of diffraction spots. The spacing and orientation of the split spots indicate a hexagonal superlattice rotated by 30° with respect to the underlying substrate and with a unit cell length of 42 ± 3 Å, consistent with the results of Barbieri *et al.* [3]. These results are also consistent with the STM images in Fig. 2. The crystallographic directions of the α-$Fe_2O_3(0001)$ substrate are indicated. (b) The fast Fourier transform (FFT) of Fig. 2(a). The FFT has been scaled and rotated to facilitate comparison with the LEED pattern shown in (a). A reciprocal unit cell corresponding to the contributions from the α phase in Fig. 2(a) has been outlined. The orientation of the spot splitting is the same as that observed in the LEED pattern in (a) and indicates a superlattice having a unit cell dimension of 35 ± 3 Å, consistent with the LEED results and direct measurements from the STM image in Fig. 2(a).

DAS reconstruction is obviously not compositionally ordered. Moreover, the faulted and unfaulted halves of the unit cell are inherently linked together, with neither being able to exist on a surface by itself.

The consistent size of the islands is very striking. We postulate that superlattice formation is driven by the lattice mismatch between oxygen sublattices. Imagine an FeO(111) island (O-O distance 3.04 Å [13]) nucleating on an α-$Fe_2O_3(0001)$ substrate (O-O distance 2.90 Å [13]) substrate. Focusing on the O sublattice, the addition of one close packed layer of larger dimension than the substrate will result in areas which have underlying hexagonal close packing, while another area has cubic close packing, and the third has oxygen atop oxygen. The first area can incorporate Fe to form an α-$Fe_2O_3(0001)$ island, albeit with a subsequent contraction of the O sublattice, while the second area can incorporate Fe to form an FeO(111) island. The third area will be unstable with respect to iron oxide formation. An idealized illustration of this O sublattice stacking effect is shown in Fig. 4. On the basis of this model, we would expect to observe similar effects on $Fe_3O_4(111)$. Indeed, our preliminary STM results do evidence behavior related to that described here.

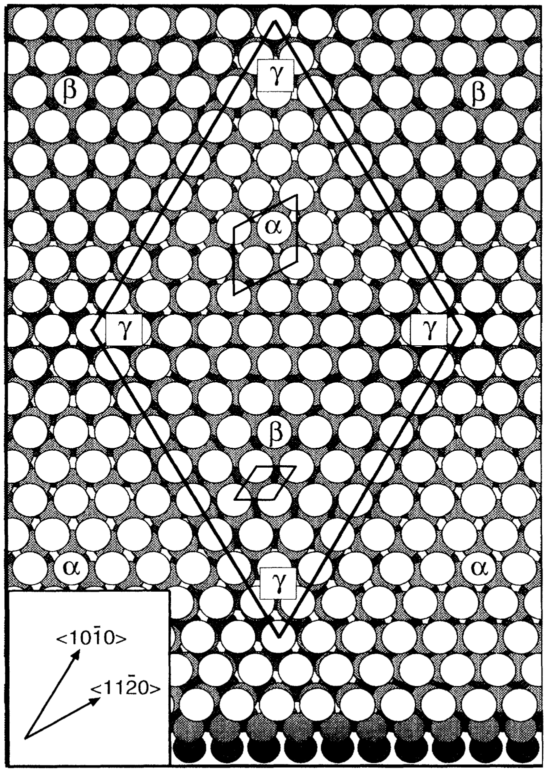

FIG. 4. Idealized model of the growth of a close packed layer onto two close packed layers of slightly smaller unit cell size. The ratio of the lattice sizes, 0.89, has been chosen for convenience. The mismatch results in areas of hexagonal close packing (α) and cubic close packing (β), as well as areas where one atom lies directly above another (γ). The unit cell of the superlattice formed by this stacking sequence is outlined, as well as those of the α and β phases. These can be compared with the unit cells indicated on the STM images in Fig. 2 after taking into account the idealized nature of the model. The crystallographic axes appropriate to the α phases are indicated.

Finally, we note two intriguing possibilities arising from this discovery. The first is that there may be other instances where LEED floreting is a result of two-dimensional superlattice formation rather than multiple scattering across an interface. This is of potential importance in studies of the growth of superlattices perpendicular to the surface. The second is related to the considerable current interest in the growth and properties of mesoscopic magnetic structures, which have potential application as high-density storage media. Bearing in mind that surface magnetic properties can be quite different to those in the bulk [15], the ordered mesoscopic structures observed here are of interest for the development of novel magnetic materials.

In conclusion, STM images of the α-$Fe_2O_3(0001)$ surface reveal a surface reconstruction consisting of a superlattice (cell length 40 ± 5 Å) of coexisting α-$Fe_2O_3(0001)$ and FeO(111) islands. We have termed this previously unanticipated phenomenon *biphase ordering*. We suggest a simple model to explain the superlattice formation based upon the oxygen lattice mismatch of the α-$Fe_2O_3(0001)$ and FeO(111) structures. Moreover, by comparing a FFT of an STM image with the corresponding LEED pattern, we have shown that in this case the associated floreting is a result of the long-range order of the superlattice and not of multiple scattering across an interface.

We are grateful to Steve Barrett for his assistance with image processing and to Brian Frederick and Walter Weaver for useful discussions. N. G. C. was supported by the Company Research Laboratory of British Nuclear Fuels plc. Other funding for this work was provided by the UK EPSRC and NERC.

---

*Also at Chemistry Department, Manchester University, Manchester M13 9PL, UK.

†To whom correspondence should be addressed.

[1] N. G. Condon *et al.,* Surf. Sci. Lett. **310**, L609 (1994).
[2] R. J. Lad and V. E. Henrich, Surf. Sci. **193**, 81 (1988).
[3] A. Barbieri, W. Weiss, M. A. Van Hove, and G. A. Somorjai, Surf. Sci. **302**, 259 (1994).
[4] W. Weiss, A. Barbieri, M. A. Van Hove, and G. A. Somorjai, Phys. Rev. Lett. **71**, 1848 (1993).
[5] R. Wiesendanger *et al.,* Science **255**, 583 (1992).
[6] R. Wiesendanger *et al.,* Z. Phys. B **86**, 1 (1992).
[7] G. Tarrach, D. Bürgler, T. Schaub, R. Wiesendanger, and H.-J. Güntherodt, Surf. Sci. **285**, 1 (1993).
[8] P. A. Johnsson, C. M. Eggleston, and MF. Hochella, Jr., Am. Mineral. **76**, 1442 (1991).
[9] C. M. Eggleston and M. F. Hochella, Jr., Am. Mineral. **77**, 911 (1992).
[10] D. H. Lindsay, *Oxide Minerals*, Short Course Notes (Mineralogical Society of America, Washington, D.C., 1976), Vol. 3, p. L66.
[11] E. Bauer, Surf. Sci. **7**, 351 (1967).
[12] Some nonstoichiometry always exists in bulk FeO[13].
[13] D. H. Lindsay, *Oxide Minerals,* Ref. [10], p. L1.
[14] A. Zangwill, in *Physics at Surfaces* (Cambridge Univ. Press, Cambridge, 1988).
[15] H. J. Elmers *et al.,* Phys. Rev. Lett. **73**, 898 (1994).
[16] D. J. Coulman, J. Wintterlin, R. J. Behm, and G. Ertl, Phys. Rev. Lett. **64**, 1761 (1990).

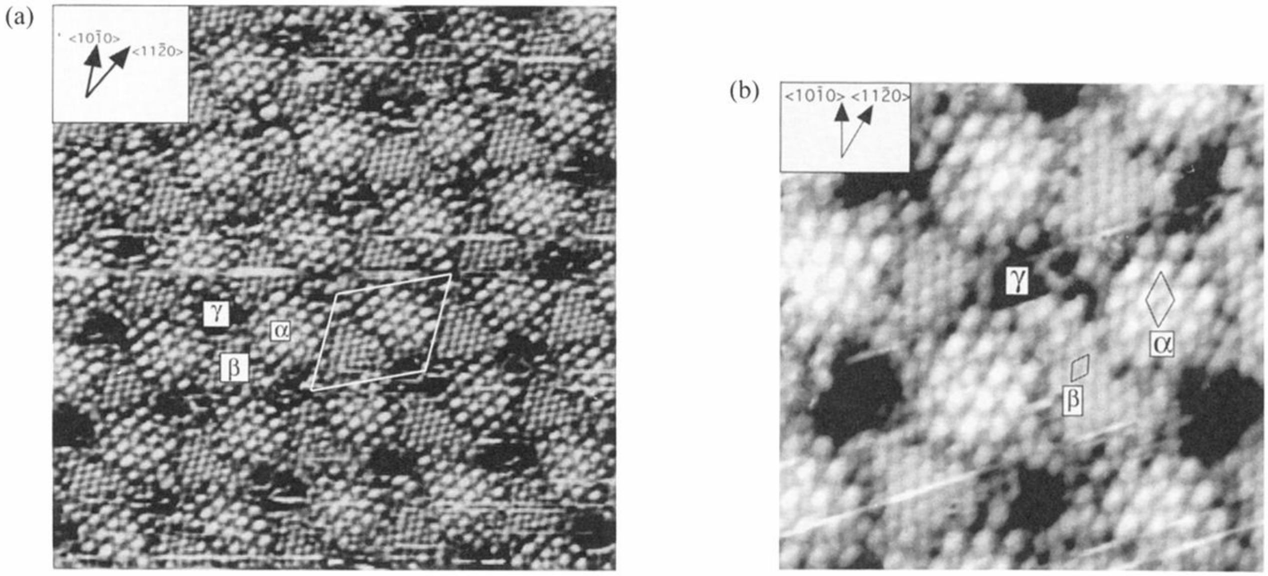

FIG. 2. (a) A 200×200 Å^2 constant current (sample bias -2 V, tunneling current 1 nA) STM image of an α-$Fe_2O_3(0001)$ surface after preparation as described in the text. This image shows two types of islands, labeled α and β, with holes at positions labeled γ. The islands are ordered, forming a hexagonal superlattice. The unit cell of the superlattice, which is indicated, has a characteristic dimension of 40 ± 5 Å and is rotated by 30° from the α-$Fe_2O_3(0001)$ lattice. Corrugations across the α and β phases are measured to be 0.5 and 0.3 Å, respectively, and γ-region holes are 2.0 ± 0.5 Å deep relative to the surrounding terraces. The crystallographic directions of the α-$Fe_2O_3(0001)$ substrate are indicated. Vertical and horizontal distances were calibrated using an image of Cu(110)-(2×1)-O which contained monatomic steps, for which the dimensions are known [16]. (b) A high resolution 80×80 Å^2 constant current (sample bias -2 V, tunneling current 1 nA) STM image of the same surface as that imaged in (a). The unit cells of the α and β phases are indicated. Atoms at the edge of the α-phase unit cell are imaged as bright features, with two weaker features just discernible within the unit cell. This contrast could arise from either an electronic effect or from surface relaxation within the island. The α-phase islands contain 18 ± 4 bright features, while the β phase contains 25 ± 6. The unit cell directions of the α-$Fe_2O_3(0001)$ substrate are shown.

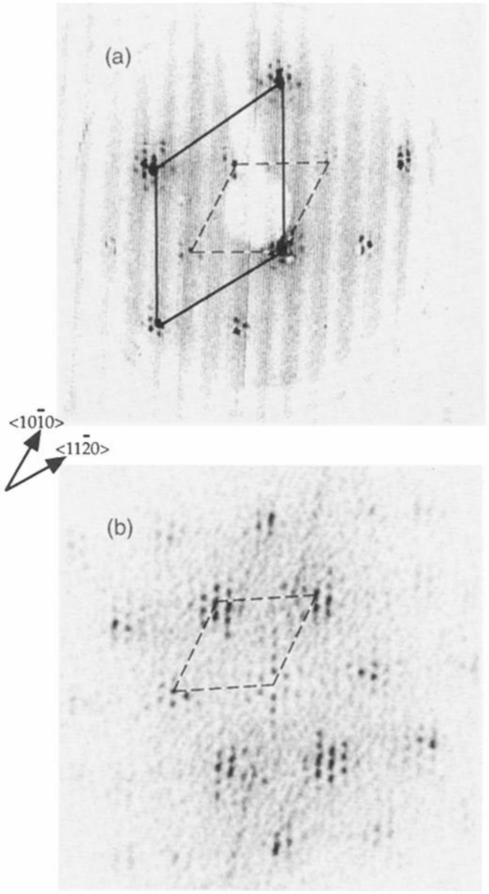

FIG. 3. (a) A LEED pattern of the surface imaged in Fig. 2, recorded at a primary beam energy of 58 eV. It was recorded off-normal incidence to reveal the zero order beam. The LEED pattern is a superposition of two symmetries, one arising from α-$Fe_2O_3(0001)$-1×1 (dashed line), the other from FeO(111)-1×1 (solid line). All the beams are floreted, being split into small hexagons of diffraction spots. The spacing and orientation of the split spots indicate a hexagonal superlattice rotated by 30° with respect to the underlying substrate and with a unit cell length of 42 ± 3 Å, consistent with the results of Barbieri *et al.* [3]. These results are also consistent with the STM images in Fig. 2. The crystallographic directions of the α-$Fe_2O_3(0001)$ substrate are indicated. (b) The fast Fourier transform (FFT) of Fig. 2(a). The FFT has been scaled and rotated to facilitate comparison with the LEED pattern shown in (a). A reciprocal unit cell corresponding to the contributions from the α phase in Fig. 2(a) has been outlined. The orientation of the spot splitting is the same as that observed in the LEED pattern in (a) and indicates a superlattice having a unit cell dimension of 35 ± 3 Å, consistent with the LEED results and direct measurements from the STM image in Fig. 2(a).